Unmanned Systems, Vol. 14, No. 4 (2026) 927–943

DOI: 10.1142/S2301385026500275

UNMANNED SYSTEMS
https://www.worldscientific.com/worldscinet/us

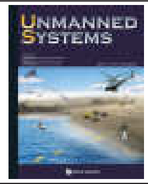

Active Anti-Disturbance Control Using Compensation Function Observer for QUAV Flight Amidst Wind and Payloads

Kuo Li [*], Guoyuan Qi [*,§,||], Kun Wang [*,¶,||], Jianbing Hu [†], Xia Li [†], Zengqiang Chen [‡]

[*]School of Control Science and Engineering, Tiangong University, Tianjin 300387, P. R. China

[†]School of Mechanical Engineering, Tiangong University, Tianjin 300387, P. R. China

[‡]School of Artificial Intelligence, Nankai University, Tianjin 300350, P. R. China

The flight of quadrotor unmanned aerial vehicles (QUAVs) faces challenges such as complex aerodynamic disturbances and time-varying payloads. To reject external disturbances and accommodate increased payloads, a control law based on a compensation function observer (CFO) and model compensation pole configuration control (CFO-based MCPCC) is proposed. The proposed control method incorporates error feedback, expected signal derivatives, disturbance estimation, and known model information, thereby achieving feedback linearization of the closed-loop system. The derivative of the reference signal is extracted using a high-order differentiator (HOD), which effectively filters out unwanted high-frequency components and improves the system's control performance. Model deviations, payload variations, and external disturbances are estimated using the CFO, and the estimated values are compensated within the control law, thereby enhancing the system's disturbance rejection capability. The utilization of known model information reduces the complexity of controller design. The proposed method is characterized not only as an active disturbance rejection control approach but also as a framework for compensating unknown dynamics. By employing Lyapunov stability theory, the asymptotic convergence of the integrated controller-observer system is demonstrated. To verify the effectiveness of the suggested control method in practice, experiments involving payload variations and wind disturbances are conducted. The results show that the proposed approach outperforms other methods in terms of payload and disturbance rejection capability. The results demonstrate that the proposed method ensures the system's tracking control performance under payload variations and wind disturbances.

Keywords: Anti-disturbances control; compensation function observer; payloads; wind disturbances; QUAV.

1. Introduction

QUAVs have garnered significant attention due to their compact size, ease of operation, and wide range of applications [1, 2]. However, QUAVs are subject to various aerodynamic disturbances and payload variations during flight operations. These challenges include enduring wind resistance, managing airflow interactions in cluster formations, and effectively transporting liquid cargo. Consequently, these factors present substantial challenges in achieving both high-precision and robust control for QUAVs.

The payload transportation capability of QUAVs has drawn considerable attention from researchers, especially for applications that require precise delivery of payloads to specific locations in disaster-affected environments, such as those impacted by earthquakes, fires, and floods. However,

Received 23 October 2024; Revised 17 March 2025; Accepted 17 March 2025; Published 7 May 2025. This paper was recommended for publication in its revised form by editorial board member, Feng Lin.
Email Addresses: [§]qiguoyuan@tiangong.edu.cn;
Email Addresses: [¶]wangkun@tiangong.edu.cn;
[||]Corresponding author.

when a QUAV carries an unknown load, both the weight and sway of the payload introduce significant challenges for accurately modeling and controlling the vehicle. To address these issues, a nonlinear tracking control method based on backstepping was developed in [3] to reduce the impact of payload sway. A comprehensive dynamic model, comprising the QUAV, cable, and payload, was proposed by Guerrero-Sánchez *et al.* to stabilize the payload's swing through interconnection and damping distribution using passive control [4]. Furthermore, considering that payload variations can affect system stability, robust control methods based on energy and interconnection and damping assignment were subsequently proposed by Guerrero-Sánchez *et al.*, effectively mitigating the impact of external disturbances [5, 6]. Wang *et al.* combined a state observer with the internal model principle to design a novel geometric tracking control method for load-carrying QUAV [7].

The flight environment of QUAVs is complex, where external aerodynamic disturbances significantly impact their performance. A wide range of control methods have been proposed to enhance the system's robustness. Zhang *et al.* proposed a fault-tolerant control method based on a prescribed performance function, which effectively enhances the system robustness and solves the problems of external disturbances and actuator failures [8, 9]. Ma *et al.* [10] proposed a nonlinear robust control strategy based on reinforcement learning to address the stabilization challenge of QUAV in the presence of wind disturbances. A nonlinear adaptive sliding mode control (SMC) was introduced to address the challenges posed by external disturbances and parameter uncertainties, thereby enhancing the anti-disturbance capability [11]. An integral backstepping SMC technique was applied to achieve robust control of the QUAV under unknown disturbance conditions [12].

When a QUAV is tasked with transporting cargo, the load can act as an external disturbance. Numerous methodologies have been proposed for QUAV operation under load and wind disturbance conditions. However, these approaches primarily employ passive control strategies, in which the controller generates a corrective signal only after an error occurs [13]. This reactive approach can lead to time delays and oscillations. Consequently, many researchers have integrated external disturbances directly into the controller design, developing various observers to estimate disturbance information and provide feedback. Commonly used disturbance observers include the extended state observer (ESO) [14], disturbance observer (DOB) [15], uncertainty and disturbance estimator [16], generalized proportional integral observer [17] and unknown input observer (UIO) [18]. Among these, ESO, DOB and UIO are particularly popular in practical applications.

An integral backstepping SMC based on ESO using an inner and outer loop control structure was recommended to improve the transient and steady-state performance of a QUAV system [19]. Zhang *et al.* [20] proposed a dual-closed-loop active disturbance rejection control (ADRC) strategy to achieve fast and accurate tracking of the target trajectory of a QUAV even in the presence of external disturbances. An SMC approach incorporating DOB with excellent control performance and effective chatter suppression was presented in [21]. Back *et al.* [22] suggested an additive inner-loop output feedback control technique based on a nonlinear DOB to improve the steady state and transient performance of the system under uncertainty and input disturbances. A tracking controller with feedforward compensation for disturbance terms, utilizing disturbance observers, was developed and demonstrated to be robust through anti-disturbance experiments [23]. Ren *et al.* [24] investigated a robust control strategy employing UDE to achieve asymptotic tracking reference and disturbance suppression within the system. Guerrero-Sánchez *et al.* [25] developed a new filtered observer-based interconnection and damping assignment-passivity based control strategy that obtained satisfactory tracking control performance. These observers are designed to mitigate the effects of unknown disturbances and model uncertainties.

The parameter selection for the nonlinear terms in the nonlinear ESO (NESO) lacks a solid theoretical foundation. As a result, tuning these parameters when applying NESO to various practical systems presents a significant challenge [26]. To address this issue, Gao [27] introduced a linear ESO, which simplifies the process of tuning controller parameters. Moreover, the ESO is a type of high-gain observer that achieves precise disturbance estimation by using relatively large parameter values. Increasing these observer parameters expands the bandwidth of detectable disturbances, but it can also introduce measurement noise [28] and peak pulse issues [29]. Ran *et al.* [30] proposed a technique for cascading the ESO based on first-order ESOs, which enhances tolerance of measurement noise by incorporating saturation in the internal variables of the observer. Qin *et al.* suggested an enhanced reduced-order ESO to suppress the peak pulse problem by reducing the order of the enhanced ESO [31]. The type of equivalent transfer function can serve as the measure for observation accuracy or criterion, and it is important to note that ESO is a Type-I system. Consequently, its estimation error for ramp signals only converges to bounded values [32]. Further, an improved ESO was developed in [32], which upgraded the type of the system to Type-II, and showed a better accuracy. Furthermore, the ESO does not utilize the system's velocity information, which could otherwise be obtained through a sensor. Qi *et al.* [33] proposed the compensation function observer (CFO) capable of achieving zero steady-state error of parabolic (Type-III) disturbance, which effectively improves the observation accuracy of disturbances.

In QUAV operations, the given signal generally has a lower frequency. Since the controller needs to utilize the derivative of this signal, a high-order differentiator (HOD) is used to filter out unreasonable high-frequency noise that may be superimposed on the desired signal [34]. Smoothing and suppressing derivative pulses in the desired signal during controller design enhances control performance, leading to smoother and more stable operation.

Based on the aforementioned challenges, this paper integrates the CFO and HOD to realize anti-disturbance control of a QUAV. The CFO is employed for estimating aerodynamic disturbances as well as managing heavy payloads encountered during flight. Meanwhile, the HOD serves to smooth out derivative pulses within desired signals.

(1) A CFO-based model compensation pole configuration control (CFO-based MCPCC) method is proposed for QUAV systems. By introducing the derivative of the reference signal, the known model, and the disturbance estimation provided by the CFO, the feedback linearization of the closed-loop system is achieved. The controller parameters can be selected using the pole placement method, where the physical interpretability of the parameters significantly reduces the difficulty of parameter tuning.

(2) Model compensation pole configuration control is characterized as an inclusive control framework where model refers to the known model being used, compensation refers to the compensation of the unknown model and disturbances, and pole configuration control refers to the selection of control gains based on pole configuration. This framework allows the CFO to be replaced with other advanced observers, and enables the control gains to be determined using alternative methods, such as backstepping or linear quadratic regulator.

(3) Despite the presence of nonlinear coupled dynamics and external disturbances, the asymptotic stability of the equilibrium point for the overall controller-observer system is established using the Lyapunov stability theorem. Comparative experimental results demonstrate the superior tracking accuracy and enhanced robustness of the proposed method.

This paper is organized as follows. The model of QUAV is presented in Sec. 2. The design of the control strategy and stability analysis is conducted in Sec. 3. In Sec. 4, experimental results and discussions are given. Section 5 summarizes this work.

2. QUAV Model and Analysis

The motion of QUAV is achieved by adjusting the motor's rotation speed in Fig. 1. m is the body mass, g is the gravity constant, l is the distance from the center of the body to the rotor. ϖ_n $(n = 1, 2, 3, 4)$ represent rotational speed of each motor. The Euler angles are expressed as $\varphi(\phi, \theta, \psi)$.

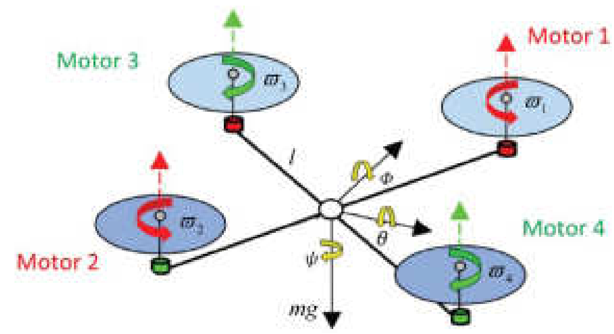

Fig. 1. Structure diagram of X-type QUAV.

The mathematical model of the X-type QUAV is given by

$$\begin{cases} \dot{v}_x = -\dfrac{1}{m}(\cos\phi\cos\psi\sin\theta + \sin\phi\sin\psi)U + f_{xu}, \\ \dot{v}_y = -\dfrac{1}{m}(\cos\phi\sin\psi\sin\theta - \sin\phi\cos\psi)U + f_{yu}, \\ \dot{v}_z = \dfrac{1}{m}(-U + mg) + f_{zu}, \end{cases} \tag{1}$$

$$\begin{cases} \ddot{\phi} = \tau_x/I_x + f_{\phi u}, \\ \ddot{\theta} = \tau_y/I_y + f_{\theta u}, \\ \ddot{\psi} = \tau_z/I_z + f_{\psi u}, \end{cases} \tag{2}$$

where v_x, v_y, v_z represent the linear velocity. I_x, I_y, I_z are the inertia of the QUAV around x, y, z. $f_{iu}(i = x, y, z)$ and $f_{ju}(j = \phi, \theta, \psi)$ are the unknown disturbances and uncertainties of each subsystem. U represents the thrust, Under hovering conditions, $U = mg$. During vertical motion, $U \neq mg$. Therefore, in the x- and y-channels of Eq. (1), we have $U = mg$. φ_d and ω_d represent the desired attitude angles and angular velocities, respectively. Define the virtual control quantities for the x, y, z, respectively, as

$$\begin{cases} u_x = \cos\phi\cos\psi\sin\theta + \sin\phi\sin\psi, \\ u_y = \cos\phi\sin\psi\sin\theta - \sin\phi\cos\psi, \\ u_z = U. \end{cases} \tag{3}$$

Based on Eq. (3), the desired angles ϕ_d, θ_d are denoted as

$$\begin{cases} \phi_d = \arcsin(u_x\sin\psi - u_y\cos\psi), \\ \theta_d = \arcsin(u_x\cos\psi + u_y\sin\psi). \end{cases} \tag{4}$$

The desired signals for the attitude subsystem are obtained by solving the inverse of the virtual control inputs u_x and u_y in the translational system. The translational motion of the body is achieved through adjustments in the attitude.

Furthermore, it is necessary to convert the torque output from each channel controller into a throttle output. This conversion facilitates control distribution, which is crucial for achieving individual motor control. The conversion relationship is as follows:

$$\begin{bmatrix} \sigma_1^2 \\ \sigma_2^2 \\ \sigma_3^2 \\ \sigma_4^2 \end{bmatrix} = \begin{bmatrix} \varepsilon_{T2\sigma} & 0 & 0 & 0 \\ 0 & \varepsilon_{\tau_x 2\sigma} & 0 & 0 \\ 0 & 0 & \varepsilon_{\tau_y 2\sigma} & 0 \\ 0 & 0 & 0 & \varepsilon_{\tau_z 2\sigma} \end{bmatrix} \begin{bmatrix} U \\ \tau_x \\ \tau_y \\ \tau_z \end{bmatrix}, \tag{5}$$

where ε_v ($v = T2\sigma, \tau_x 2\sigma, \tau_y 2\sigma, \tau_z 2\sigma$) are known as the power coefficients. If the magnitude is selected excessively, it will induce oscillatory behavior in the quadrotor. Conversely, if the magnitude is insufficient, it can result in the quadrotor experiencing loss of stability. Hence, the careful determination of the power coefficient is intricately associated with the control performance of the quadrotor.

To facilitate controller design and analysis, the following assumptions are made.

Assumption 1 ([35]). The QUAV is considered a symmetric rigid body, implying uniform mass distribution and axial symmetry, with its inertia matrix being diagonal.

A small QUAV is characterized by a light structure and a rigid structure, which allows deformations to be neglected, thus satisfying the rigid body assumption. Assumption 1 is a common assumption for constructing QUAV models

Assumption 2 ([36]). The disturbance is expressed as a third-order infinitesimal function. This implies that the unknown function can be an arbitrary combination of constant, linear and quadratic functions.

Based on the Taylor expansion theory, the contribution of higher-order derivative terms decreases rapidly as the expansion order increases. Furthermore, the typically small sampling interval further diminishes the influence of higher-order terms on the overall expansion. To enhance the rigor of the proof, the higher order signals of the disturbances are neglected.

Assumption 3. The reference input signal is a second-order differentiable and the third-order infinitesimal function. In the flight of the QUAV, the reference signal is provided by the remote controller, usually in the form of step or ramp signals.

The step reference signal is passed through a second-order low-pass filter, transforming the step signal into a second-order differentiable signal. Moreover, step signals are prone to overshoot. In engineering applications, it is common practice to apply signal smoothing to input signals, such as using filters for smoothing, before feeding the smoothed signal into the controller.

3. Robust Controller Design and Stability Analysis

3.1. *Problem description*

Based on the model analysis in Sec. 2, Eq. (1) describes the velocity loop system, which is a first-order system, with the left-hand side representing the first derivative of velocity. Equation (2) describes the attitude loop system as a second-order system, with the left-hand side representing the second derivative of the attitude angle.

(1) First-order velocity system: The general form of the velocity loop system in Eq. (1) can be written as

$$\dot{y}_i = f_{ik} + f_{iu} + b_i u_i, \tag{6}$$

where y_i is the output, representing the velocity. f_{ik} and f_{iu} represent the known dynamics and lumped disturbances, respectively. $f_{xk} = f_{yk} = 0$, $f_{zk} = g$. b_i is a constant, with $b_x = b_y = -g$ in the x- and y-channels, with $b_z = -1/m$ in the z-channel. u_i the control input.

(2) Second-order attitude system: The general form of the attitude loop system in Eq. (2) can be expressed as

$$\ddot{y}_j = f_{ju} + b_j u_j, \tag{7}$$

where y_j is the output, representing the attitude angle. f_{ju} represents external disturbances and uncertainties. b_j is the reciprocal of the I_j. u_j is the control input, and $u_j = \tau_j$.

Many systems can be expressed in the general form of Eqs. (6) and (7), including QUAV systems, circuit systems, etc. To extend the applicability of the controller, Eqs. (1) and (2) are expressed as Eqs. (6) and (7).

3.2. *Design of controller*

A model compensation pole configuration control (MCPCC) method based on compensation function observer (CFO) is illustrated in Fig. 2. Model refers to the feedforward of known information into the control law. Compensation refers to the incorporation of external disturbances, as estimated by the CFO, into the control laws. The control parameters are selected by the pole configuration method. The high-order differentiator (HOD) is utilized to extract high-order information from the reference signal. For these reasons, this approach achieves stable control of the QUAV.

(1) Control law for first-order systems: The control laws are developed as a cascade control approach including proportional control and a second-order MCPCC. The design process consists of two steps.

Step 1. The position loop is controlled by using the following proportional control:

$$v_{ip} = k_{ip}(x_{i1d} - x_{i1}), \tag{8}$$

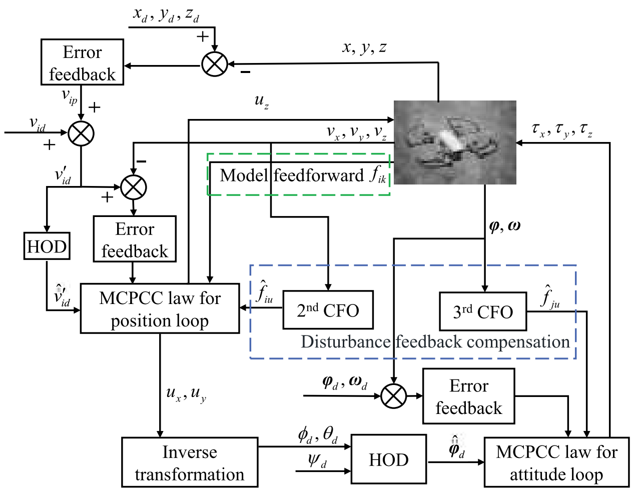

Fig. 2. Configuration diagram of system MCPCC.

where k_{ip} is a proportional gain constant, x_{i1d} the desired position, and x_{i1} the current position. The purpose of the variable v_{ip} is to decrease the position error through proportional control. Meanwhile, the proportional control output v_{ip} and the speed signal provided by the remote control v_{id} feed forward to the inner loop speed controller, i.e.

$$v'_{id} = v_{ip} + v_{id}, \tag{9}$$

where v'_{id} is the total desired velocity.

Step 2. Constructing a second-order MCPCC control law. The translational dynamics equation (1) can be transformed into

$$\dot{v}_i = f_{ik} + f_{iu} + b_i u_i, \tag{10}$$

where v_i represents velocity signal. f_{iu} can be obtained through the observer and feedback to the control law to counteract the adverse effects of unknown disturbances. f_{ik} represents the known component of the model, and $f_{ik} = [0, 0, g]^{\mathrm{T}}$.

The velocity error variable e_{i1} is defined as

$$e_{i1} = v'_{id} - v_i. \tag{11}$$

The design error converges exponentially as follows:

$$\dot{e}_{i1} = -k_{iv} e_{i1}, \tag{12}$$

where k_{iv} is the gain coefficient.

The control law can be developed as

$$u_i = \frac{1}{b_i}(k_{iv} e_{i1} + \dot{v}'_{id} - \hat{f}_{iu} - f_{ik}), \tag{13}$$

where $\hat{f}_{iu}$ represents the estimate of f_{iu}.

(2) Control law design for second-order systems: The error of the system is defined as

$$\begin{cases} e_{j1} = x_{j1d} - x_{j1}, \\ e_{j2} = x_{j2d} - x_{j2}, \end{cases} \tag{14}$$

where e_{j1}, e_{j2} are the state errors, x_{j1d}, x_{j2d} the desired state variables, and x_{j1}, x_{j2} the state variables. According to Eqs. (7) and (14), the derivation of Eq. (14) is given

$$\begin{cases} \dot{e}_{j1} = \dot{x}_{j1d} - \dot{x}_{j1} = e_{j2}, \\ \dot{e}_{j2} = \dot{x}_{j2d} - \dot{x}_{j2} = \dot{x}_{j2d} - (f_{ju} + b_j u_j). \end{cases} \tag{15}$$

The design error converges exponentially as follows:

$$\begin{bmatrix} \dot{e}_{j1} \\ \dot{e}_{j2} \end{bmatrix} = \begin{bmatrix} 0 & 1 \\ -k_{j1} & -k_{j2} \end{bmatrix} \begin{bmatrix} e_{j1} \\ e_{j2} \end{bmatrix}, \tag{16}$$

where k_{j1}, k_{j2} are the parameters to be chosen. One becomes

$$\dot{\mathbf{e}}_j = \mathbf{A}_j \mathbf{e}_j, \tag{17}$$

where

$$\mathbf{A}_j = \begin{bmatrix} 0 & 1 \\ -k_{j1} & -k_{j2} \end{bmatrix}, \quad \mathbf{e}_j = \begin{bmatrix} e_{j1} \\ e_{j2} \end{bmatrix}.$$

Therefore, the MCPCC law can be written as

$$u_j = \frac{1}{b_j}(k_{j1} e_{j1} + k_{j2} e_{j2} + \ddot{x}_{j1d} - \hat{f}_{ju}). \tag{18}$$

In Eq. (18), $\hat{f}_{ju}$ is the estimate of f_{ju}, compensating the model uncertainties and external disturbance, this approach is called model compensation control. The system is asymptotically stable if $\mathbf{A}_j$ merely has eigenvalues with negative real parts.

Thus, k_{j1}, k_{j2} can be configured as follows:

$$|s\mathbf{I} - \mathbf{A}_j| = (s + a_1)(s + a_2) = 0, \tag{19}$$

where a_1, a_2 are the to-be-selected eigenvalues.

Remark 1. Disturbance issues were addressed through the integration of fractional-order sliding mode control with barrier function theory in [37]. However, this control approach exhibits computational complexity and challenges in parameter tuning. The proposed control laws feature fewer parameters and possesses clear physical interpretations.

3.3. *Compensation function observer design*

If the controller fails to consider the lumped disturbances f_{iu}, f_{ju}, it may result in weak robustness in control performance and even potential instability. Second-order and third-order CFOs are used to observe the unknown disturbances and unmodeled dynamics of the system for the above first-order and second-order QUAV systems, respectively. The two CFOs of different orders are independent of each other. Moreover, the third-order CFO utilizes an additional system state x_2, rather than merely introducing an extra parameter, as compared to the second-order CFO.

(1) Second-order CFO [33]: The second-order CFO is written as

$$\begin{cases} \dot{z}_{i1} = z_{i2} + l_i e_{io1} + b_i u_i + f_{ik}, \\ \dot{z}_{i2} = \lambda_i l_i e_{io1}, \\ \hat{f}_{iu} = z_{i2} + l_i e_{io1}, \end{cases} \tag{20}$$

where z_{i1}, z_{i2} are the observation values of x_{i1}, f_{iu}. λ_i and l_i are the constants. Define the estimation error as $e_{io1} = x_{i1} - z_{i1}$. The error analysis is shown in [33]. $\hat{f}_{iu}$ in the control law of Eq. (13) represents the estimated value of the disturbance $\hat{f}_{iu}$ by the observer in Eq. (20).

The equivalent open-loop error transfer function is expressed as

$$G_{\text{CFO}}^{\text{2nd}}(s) = \frac{l_i s + \lambda_i l_i}{s^2}. \tag{21}$$

The corresponding characteristic equation of Eq. (21) is written as

$$s^2 + l_i s + \lambda_i l_i = (s + \omega)(s + \gamma\omega) = 0, \tag{22}$$

where γ is a positive constant. A larger γ means that the two poles are further apart. Let $\gamma = 3$ and we have

$$l_i = 4\omega, \quad \lambda_i = 3\omega/4, \tag{23}$$

where ω is a constant. ω has a clear physical meaning: it represents the location of the desired system poles on the negative real axis. The larger the value of ω, the higher the estimation accuracy, and the faster the transient response. However, too large a parameter may result in peak pulsing and oscillations. Thus, the selection of ω must also consider the initial oscillation.

(2) Third-order CFO: The third-order CFO is given as

$$\begin{cases} \dot{z}_{j1} = z_{j2}, \\ \dot{z}_{j2} = z_{j3} + \mathbf{L}\mathbf{e}_{jo} + b_j u_j, \\ \dot{z}_{j3} = \lambda_j \mathbf{L}\mathbf{e}_{jo}, \\ \hat{f}_{ju} = z_{j3} + \mathbf{L}\mathbf{e}_{jo}, \end{cases} \tag{24}$$

where z_{j1}, z_{j2}, z_{j3} are the states of observer, $\mathbf{L} = [l_{j2}, l_{j1}]$ the gain matrix. Define the estimation error as $\mathbf{e}_{jo} = [e_{jo1}, e_{jo2}]^{\mathrm{T}} = [x_{j1} - z_{j1},\ x_{j2} - z_{j2}]^{\mathrm{T}}$. $\hat{f}_{ju}$ in the control law of Eq. (18) represents the estimated value of the disturbance $\hat{f}_{ju}$ by the observer in Eq. (24).

In Eq. (24), the high-precision estimation capability of the CFO stems from: (1) the utilization of new system information x_2; (2) its pure derivative structure, where $\dot{z}_{j1} = z_{j2}$. Therefore, the CFO parameters do not require high-gain tuning like in ESO. The high-precision estimation of the ESO requires the selection of large bandwidth parameters, which can amplify system noise. The parameter tuning of the CFO is based on the pole placement method, which endows the parameters with clearer physical significance and makes them easier to adjust.

Lemma 1 ([33]). *For the second-order system, when f_{ju} satisfies Assumption 2, the designed CFO is asymptotic stable and the estimation is convergent, i.e.* $\lim_{t\to\infty} \hat{f}_{ju} = f_{ju}$.

The error and convergence analyses are shown in [33].

To estimate f_{ju}, many disturbance observers have been developed. The ESO is a popular one [14], however, the estimation accuracy of f_{ju} is low, as indicated in [32] where the error analysis is provided.

To illustrate the superiority of the proposed method more effectively, we introduce the improved extended state observer (IESO). The selection criterion for observer parameters emphasizes stability and optimal performance. Given the inherent complexity associated with tuning multiple parameters, a unification approach is adopted to consolidate them into a single parameter. As derived in [32, 33], the general equation of the equivalent open-loop error transfer function for the third-order IESO and CFO is expressed as follows:

$$G_{\text{IESO}}(s) = \frac{l_{e2}s + l_{e3}}{s^2(s + l_{e1})}, \tag{25}$$

$$G_{\text{CFO}}(s) = \frac{l_{c1}s^2 + (\lambda l_{c1} + l_{c2})s + \lambda l_{c2}}{s^3}, \tag{26}$$

where $l_{e1},\ l_{e2},\ l_{e3},\ l_{c1},\ l_{c2},\ \lambda$ are positive constants.

From Eqs. (25) and (26), their corresponding characteristic equations, respectively, can be obtained as

$$s^3 + l_{e1}s^2 + l_{e2}s + l_{e3} = 0, \tag{27}$$

$$s^3 + l_{c1}s^2 + (\lambda l_{c1} + l_{c2})s + \lambda l_{c2} = 0. \tag{28}$$

To make stable for the observers, let the characteristic equation of Eqs. (27) and (28) have negative real parts:

$$\begin{aligned} &s^3 + l_{e1}s^2 + l_{e2}s + l_{e3} \\ &\quad = (s + \omega_e)(s + \alpha\omega_e)^2 = 0, \end{aligned} \tag{29}$$

$$\begin{aligned} &s^3 + l_{c1}s^2 + (\lambda l_{c1} + l_{c2})s + \lambda l_{c2} \\ &\quad = (s + \omega_c)(s + \alpha\omega_c)^2 = 0, \end{aligned} \tag{30}$$

where α is a positive constant and satisfies $\alpha \geq 4$ for allocating the solutions $-\omega_e, -\omega_c$ as the dominant poles. Thus, $l_\kappa(\kappa = e_1,\ e_2,\ e_3,\ c_1,\ c_2)$ and λ can be obtained by Eqs. (29) and (30), we have

$$l_{e1} = (2\alpha + 1)\omega_e, \quad l_{e1} = (\alpha + 2)\alpha\omega_e^2, \quad l_{e1} = \alpha^2\omega_e^3, \tag{31}$$

$$l_{c1} = (2\alpha + 1)\omega_c,$$

$$l_{c2} = \frac{\alpha\omega_c^2 \mp \omega_c^2\sqrt{(\alpha^3(\alpha-4))}}{2} + \alpha^2\omega_c^2/2, \quad (32)$$

$$\lambda_j = \frac{(\alpha\omega_c^2 \pm \omega_c^2\sqrt{(\alpha^3(\alpha-4))}/2 + \alpha^2\omega_c^2/2)}{(\omega + 2\alpha\omega_c)}.$$

Let $\alpha = 4$, we have

$$l_{e1} = 9\omega_e, \quad l_{e1} = 24\omega_e^2, \quad l_{e1} = 16\omega_e^3, \quad (33)$$

$$l_{c1} = 9\omega_c, \quad l_{c2} = 12\omega_c^2, \quad \lambda_j = 4\omega_c/3. \quad (34)$$

Therefore, parameters of the IESO and the CFO are designed as $\omega_e = \omega_c$.

3.4. *Introduction of HOD*

In real flight scenarios, the reference input signal of a QUAV generally exhibits smooth variations with minor fluctuations. However, high-frequency noise may affect this reference signal, causing rapid oscillations in its second-order derivatives. These oscillations appear within the control law described in Eq. (18). Thus, smoothing the signal becomes necessary. To address this issue, an HOD is employed to extract higher-order derivatives from the input signal.

The general form of third-order HOD is expressed as

$$\begin{cases} \dot{z}_{h1} = z_{h2} + h_1(y_d - z_{h1}), \\ \dot{z}_{h2} = z_{h3} + h_2(y_d - z_{h1}), \\ \dot{z}_{h3} = h_3(y_d - z_{h1}), \end{cases} \quad (35)$$

where z_{h1}, z_{h2} are the observed states of the system with the form of Eqs. (6) and (7) when $u = 0$. $\mathbf{h} = [h_1, h_2, h_3]$ are the positive constants to be chosen. For estimating the first-order and second-order derivative of y_d, $\mathbf{h}$ includes $\mathbf{h}_i = [h_{i1},\ h_{i2}]$ and $\mathbf{h}_j = [h_{j1},\ h_{j2},\ h_{j3}]$. y_d is the referenced signal. The HOD aims to estimate the derivatives of y_d and filter out clutter. The parameter selection method is

$$s^2 + h_{i1}s + h_{i2}s = (s + c_i)(s + 3c_i) = 0, \quad (36)$$

$$s^3 + h_{j1}s + h_{j2}s + h_{j3} = (s + c_j)^3 = 0, \quad (37)$$

where c_i and c_j are the poles to be selected.

The output equation of HOD is expressed as

$$\begin{cases} \hat{y}_d = z_{h1}, \\ \hat{\dot{y}}_d = \dot{z}_{h1} = z_{h2} + h_1(y_d - z_{h1}), \\ \hat{\ddot{y}}_d = \dot{z}_{h2} = z_{h3} + h_2(y_d - z_{h1}), \end{cases} \quad (38)$$

where $\hat{y}_d, \hat{\dot{y}}_d, \hat{\ddot{y}}_d$ are the estimates of the signal of each order of derivative of y_d, respectively.

Lemma 2 ([38]). *The HOD can achieve zero error convergence for its second-order differential when satisfies Assumption* 3.

Therefore, based on Eqs. (20), (24) and (38), the control laws of Eqs. (13) and (18) are rewritten as

$$u_i = 1/b_i(k_{iv}e_{i1} + \hat{\dot{v}}'_{id} - \hat{f}_{iu} - f_{ik}), \quad (39)$$

$$u_j = 1/b_j(k_{j1}e_{j1} + k_{j2}e_{j2} + \hat{\ddot{x}}_{j1d} - \hat{f}_{ju}), \quad (40)$$

where $\hat{f}_{iu}$ and $\hat{f}_{ju}$ are estimates of the disturbances obtained from Eqs. (20) and (24), respectively. $\hat{\dot{v}}'_{id}$ and $\hat{\ddot{x}}_{j1d}$ denote the estimates of $\dot{v}'_{id}$ and $\ddot{x}_{j1d}$, respectively.

Remark 2. Compared to the classical ADRC, the proposed method differs in the following aspects: (1) by introducing the second-order derivative of the desired signal $\hat{\ddot{x}}_{j1d}$, the closed-loop error equation satisfies Eqs. (15) and (17), achieving feedback linearization; (2) disturbances are estimated with high precision using the CFO method and are fed forward into the controller to counteract the disturbances, $\hat{f}_{iu}$ and $\hat{f}_{ju}$; (3) full utilization of the known model information $\hat{f}_{ik}$; (4) the pole placement method is employed to select the control parameters, reducing the difficulty of parameter tuning.

The proposed control is shown in Fig. 3. The model feedforward information f_k and the disturbance compensation f_{uk} together constitute the complete model of the system; y_r is the reference signal, and its high-order signals can be extracted by the designed differentiator; the state error feedback module is employed to stabilize the closed-loop system. The differentiator, state and disturbance observer, and state error feedback module in the framework can be designed differently according to practical requirements.

In contrast to the use of multiple disturbance observers in [13], the method proposed only requires a single observer, significantly reducing the complexity of practitioners' work.

Under the same simulation time and hardware setup, the computational complexity of the proposed CFO-based MCPCC method is quantified by calculating the simulation run time. The average run times for CFO-based MCPCC and the nonlinear model predictive control (NLMPC) from [39] are 1.6754 s and 3.5816 s, respectively. The results clearly show that the proposed method has a significantly lower computational complexity compared to NLMPC. Since the structure of the proposed method is similar to that of classical ADRC, its computational complexity is comparable.

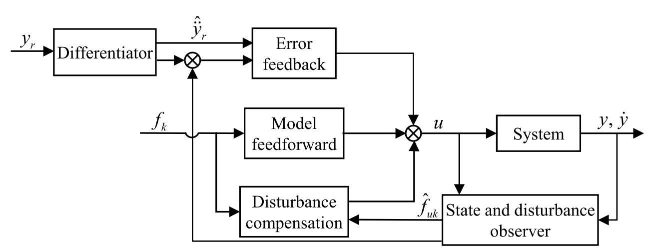

Fig. 3. Model compensation pole configuration control block diagram.

3.5. *Stability proof of the close-loop system*

Theorem 1. *When f_{ju} and y_{jd} satisfy Assumptions 2 and 3, respectively, the developed control law of Eq. (40) can make the QUAV system achieve trajectory tracking while guaranteeing attitude stability. Then, if Constants k_{j1} and k_{j2} can be properly selected, the closed-loop system is asymptotically stable.*

Proof. A Lyapunov function can be defined as follows:

$$V_e = (k_{j1} + k_{j1}^2 + k_{j2}^2)e_{j1}^2 + 2k_{j2}e_{j1}e_{j2} + (1 + k_{j1})e_{j2}^2, \tag{41}$$

where $e_{j1} = x_{j1d} - x_{j1}$, $e_{j2} = x_{j2d} - x_{j2}$. In the process of proof, to simplify notation, subscripts denoted by 'j' are omitted. We then have

$$\begin{aligned} V_e &\geq (k_1 + k_1^2 + k_2^2)e_1^2 - k_2^2e_1^2 - e_2^2 + (1 + k_1)e_2^2 \\ &\geq (k_1 + k_1^2)e_1^2 + k_1e_2^2 \geq 0. \end{aligned} \tag{42}$$

Hence, $V_e \geq 0$ at $k_1 > 0$. The derivative of Eq. (41) yields

$$\begin{aligned} \dot{V}_e = {} & 2(k_1 + k_1^2 + k_2^2)e_1e_2 + 2k_2e_2^2 \\ & + 2k_2e_1\dot{e}_2 + 2(1 + k_1)e_2\dot{e}_2. \end{aligned} \tag{43}$$

Letting $\dot{V}_e = 2(k_1 + k_1^2 + k_2^2)e_1e_2 + 2k_2e_2^2 + M + N$, one holds

$$\begin{cases} M = 2k_2e_1\dot{e}_2, \\ N = 2(1 + k_1)e_2\dot{e}_2. \end{cases} \tag{44}$$

Combining Eqs. (40) and (44), one gets

$$\begin{cases} M = 2k_2e_1(e_f + e_h - k_1e_1 - k_2e_2), \\ N = 2(1 + k_1)e_2(e_f + e_h - k_1e_1 - k_2e_2), \end{cases} \tag{45}$$

where $e_f = \hat{f}_u - f_u$, $e_h = \ddot{x}_{1d} - \hat{\ddot{y}}_{1d}$. Under Lemmas 1 and 2, the estimation errors of f_u by the CFO and $\ddot{x}_{1d}$ by the HOD converge to 0, i.e. $\lim_{t\to\infty} e_f = 0$, $\lim_{t\to\infty} e_h = 0$. We have

$$\begin{cases} M = -2k_1k_2e_1^2 - 2k_2^2e_1e_2, \\ N = -2k_1e_1e_2 - 2k_2e_2^2 - 2k_1^2e_1e_2 - 2k_1k_2e_2^2. \end{cases} \tag{46}$$

From Eq. (46), Eq. (43) can be rewritten as

$$\dot{V}_e = -2k_1k_2(e_1^2 + e_2^2) \leq 0. \tag{47}$$

If and only if $e_1 = 0$, $e_2 = 0$, $V_e \leq 0$. Clearly, $\dot{V}_e$ is bounded. When $e_1 \to 0$ and $e_2 \to 0$, $\dot{V}_e \to 0$. According to Barbalat lemma [40], it can be inferred that the system demonstrates asymptotic stability. The proof is completed. □

Table 1. Structural parameters of the body.

Wind tunnel experiment		Other types of experiments	
Parameters	Value	Parameters	Value
m	1.072	m	2.125
l	0.1	l	0.225
$I_x = I_y$	0.0039	$I_x = I_y$	0.02145
I_z	0.0059	I_z	0.03223

4. Experimental Setup and Results

To verify the robustness of the proposed method, payload and anti-wind disturbance experiments are designed. The structural parameters of the QUAV used for each experiment are indicated in Table 1.

Smaller wheelbase QUAV is used in experiments on wind tunnel due to limitations in the inner diameter of the wind tunnel. A motion capture system is employed to measure the real-time position information of the QUAV and send it to the controller via WIFI. The overall schematic is shown in Fig. 4.

The parameters of each channel of the attitude loop are chosen to be consistent with the roll, and the parameters of each channel of the position loop are chosen to be consistent with the vertical. The IESO-based MCPCC and CFO-based MCPCC detailed parameter settings are illustrated in Table 2.

The control law of LADRC is

$$u_{\mathrm{LADRC},i} = \frac{(k_{A,2}(k_{A,1}(y_{id} - y_i) - v_i) - \hat{f}_{\mathrm{ESO},i})}{b_i}, \tag{48}$$

where $k_{A,1} = 0.3$, $k_{A,2} = 2$.

The parameters of ESO are $\beta_1 = 14$, $\beta_2 = 49$.

The parameter definitions for the classical nonlinear active disturbance rejection control (NLADRC) and NLMPC are provided in [14, 39], respectively. The corresponding parameter values are given in Table 3.

The power coefficients for the five methods are listed in Table 4.

Note that the power coefficients equation (5) in the horizontal for LADRC, NLADRC, NLMPC and IESO-based MCPCC are 2.79 times higher than those for CFO-based MCPCC. Suitable power parameters can enhance the control performance of the controller. When the power parameter is too large, it can cause the QUAV to shake violently, while a small power parameter may result in weaker control.

4.1. *Experiments with payload*

In the payload experiments, the following experiments are included: (1) A 0.2 kg weight is suspended on the side of the QUAV to complete the attitude tracking experiment; (2)

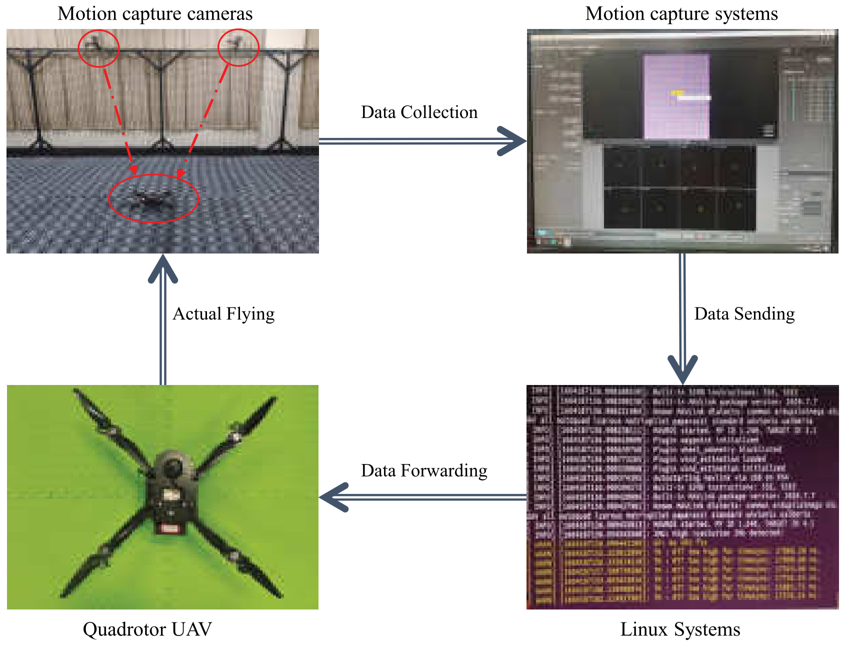

Fig. 4. Data acquisition and transmission in motion capture systems.

Table 2. Selection of control parameters.

Parameters	Value $x,\ y,\ z$	Parameters	Value ϕ, θ
k_{iv}	6, 6, 6	k_{j1}	16, 16
c_i	5, 5, 5	k_{j2}	16, 16
ω	3, 3, 3	c_j	10, 10
k_{ip}	0.5, 0.5, 5.5	$\omega_e = \omega_c$	2.3, 2.3

Table 3. Selection of parameters.

NLADRC		NLMPC	
Parameters	Value	Parameters	Value
$r_{\mathrm{TD}},\ h_{\mathrm{TD}},\ c_{\mathrm{NLSEF}}$	100, 1, 6	N	10
$\beta_{01},\ \beta_{02},\ \beta_{03}$	45, 600, 2000	$u_{\min}, u_{\max}$	−5, 5
$r_{\mathrm{NLSEF}},\ h_{\mathrm{NLSEF}}$	200, 25	Q	diag{1, 0.5}
$d_{\mathrm{ESO}},\ h_{\mathrm{ESO}}$	0.01, 1	R	0.1

three-dimensional path tracking experiment with a payload-equipped QUAV.

4.1.1. *Attitude tracking experiment with payload*

A weight of 0.2 kg is affixed to the midpoint of the line connecting motors 1 and 4 of the QUAV using a thin, non-elastic wire measuring 0.4 m in length.

The IESO-based MCPCC is illustrated in Fig. 5(a) which demonstrates a significant steady-state error, with a mean absolute error (MAE) of 6.1083, as depicted in Fig. 6(a). On the contrary, the CFO-based control exhibits a stable and accurate roll angle control (Fig. 5(b)) with an MAE of 0.6447 (Fig. 6(b)). In terms of mean error, the CFO-based MCPCC surpasses the IESO-based MCPCC by 89.45%, indicating its resilience to disturbances.

Table 4. Selection of power coefficients.

The other methods		CFO-based MCPCC	
Parameters	Value	Parameters	Value
$T2\sigma$	0.026	$T2\sigma$	0.026
$\tau_x 2\sigma = \tau_y 2\sigma$	0.456	$\tau_x 2\sigma = \tau_y 2\sigma$	0.163
$\tau_z 2\sigma$	1.229	$\tau_z 2\sigma$	1.229

4.1.2. *Altitude tracking experiments with payload*

In Fig. 7, a 0.5 kg weight is suspended below the QUAV using a 0.15 m long string.

Figure 8 shows the three-dimensional path tracking performance of LADRC, NLADRC, NMPC, IESO-based MCPCC and CFO-based MCPCC under varying load conditions. From Fig. 8(a), it is evident that both the LADRC and IESO-based MCPCC methods exhibit significant trajectory deviations, with root mean square error (RMSE) values of 0.2367 and 0.0805, respectively. Similarly, as illustrated in Fig. 8(b), the tracking trajectories of the NLADRC and NMPC methods also demonstrate significant deviations, with RMSE values of 0.2553 and 0.1221, respectively. In contrast, the proposed CFO-based MCPCC achieves markedly superior tracking accuracy, yielding the smallest RMSE of 0.0452.

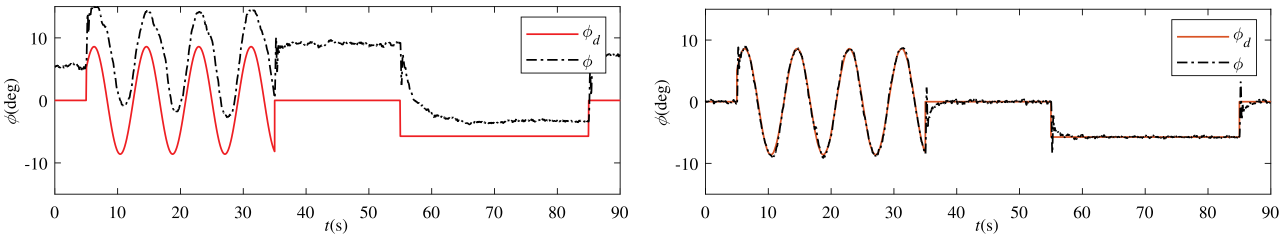

(a) (b)

Fig. 5. IESO-based MCPCC and CFO-based MCPCC: Tracking task.

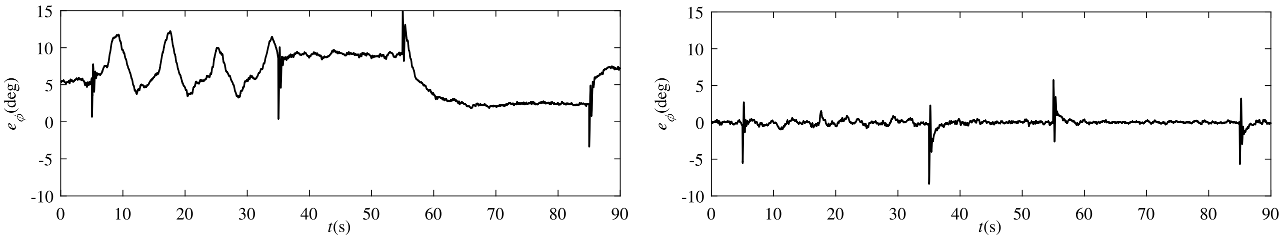

(a) (b)

Fig. 6. IESO-based MCPCC and CFO-based MCPCC: Tracking error.

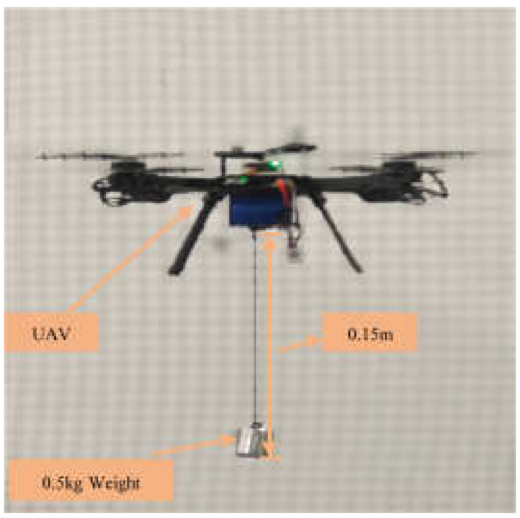

Fig. 7. Altitude tracking experiments with unknown loads.

These results clearly indicate that, under identical payload conditions, the proposed method outperforms the other methods in terms of tracking accuracy.

Remark 3. In the load enhancement experiment documented in [41], the weight of the load accounts for approximately 18.60% of the QUAV's total weight. However, the method proposed in this paper carries a load equivalent to approximately 23.53% of the QUAV's total weight.

4.2. *Design of experiments for wind disturbance*

To verify the anti-disturbance performance of the proposed method, the following experiments are conducted: (1) Stabilization experiment in a small wind tunnel. (2) Fixed-point hovering anti-disturbance experiment. (3) Three-dimensional trajectory tracking experiment under variable wind conditions. (4) Three-dimensional path tracking experiment under constant wind conditions (4 m/s).

4.2.1. *Attitude stabilization in a small wind tunnel*

To accommodate the limited inner diameter of the wind tunnel, a QUAV with a wheelbase of $l = 0.1$ m is employed to conduct the stabilization experiment. The structure of the small wind tunnel is depicted in Fig. 9. Its primary components encompass an electric motor, fan blade, culvert, and three-dimensional force sensor. The QUAV is securely positioned on a test stand within the wind tunnel, aligning the wind direction along the x-axis of the QUAV. In Fig. 10, the wind levels and their corresponding speeds are depicted, with the wind speed data being derived from the averaging of multiple data sets, thereby ensuring a comprehensive representation.

The control performance of the QUAV is illustrated in Fig. 11. Under level 1 or level 2 wind conditions, no significant difference is observed in the pitch response between the two methods. However, from Fig. 11(a), under level 3 conditions, the IESO-based MCPCC exhibits significant oscillations

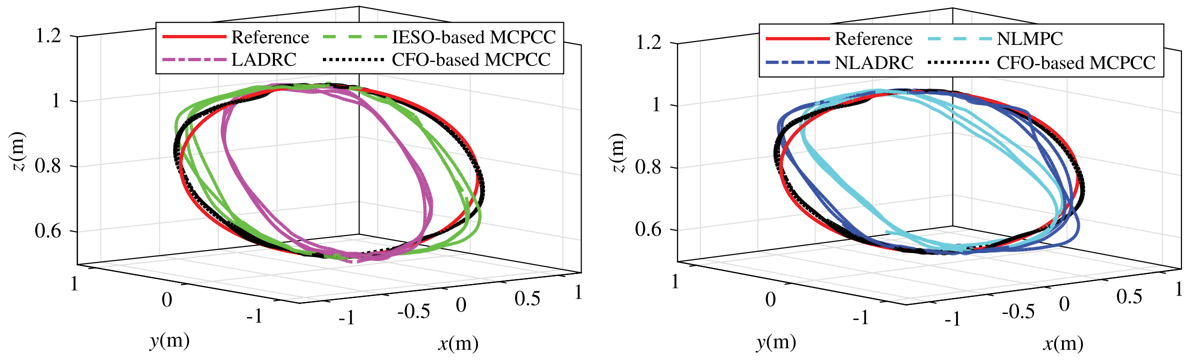

(a) Test 1

(b) Test 2

Fig. 8. Altitude tracking experiments with unknown loads.

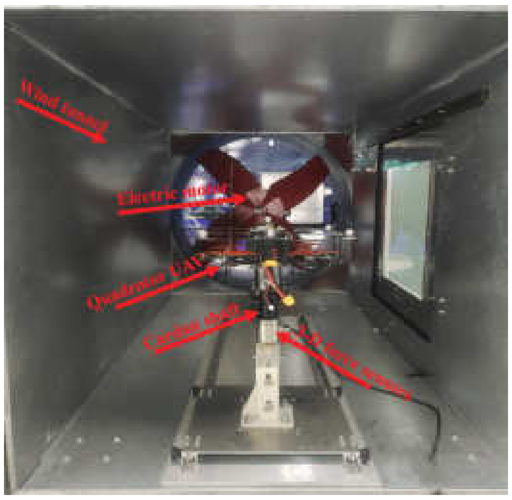

Fig. 9. Structural components of the small wind tunnel.

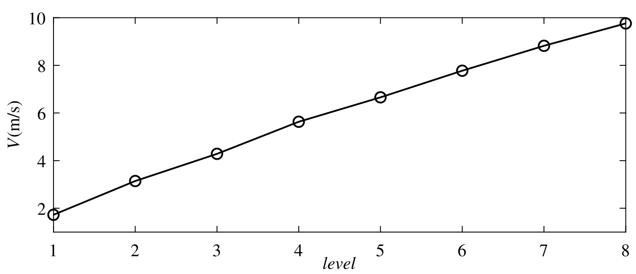

Fig. 10. Wind levels and corresponding wind speeds.

which eventually result in the destabilization of the QUAV. For safety considerations, the QUAV operations are suspended. In Fig. 11(b), the CFO-based MCPCC exhibits a similar attitude response to that of level 3, even when subjected to level 4, despite having adjusted the airflow to 6 m/s. It is only under level 5 that the attitude response of the CFO-based MCPCC resembles the response of the IESO-based MCPCC under level 3.

Figure 12 illustrates the lift force generated by the quadrotor as measured by the force sensor. To ensure fairness in the comparative experiments, the throttle of the remote controller is adjusted to a consistent position in both sets of experiments to achieve an equal level of lift force. Since the control performance of the two methods is comparable at levels 1 and 2, their lift forces exhibit consistent behavior. From Fig. 13, the attitude response performance of both methods is comparable at levels 1 and 2 with identical throttle inputs. Consequently, the vertical lift forces are similar in Fig. 12. It is noteworthy that the power coefficients utilized in Figs. 11 and 12 differ between the two methods. The IESO-based MCPCC utilizes twice the number of power coefficients compared to the CFO-based MCPCC. The CFO-based MCPCC employs a power factor of $\tau_{x2\sigma} = \tau_{y2\sigma} = 0.163$. Despite having a smaller power coefficient, the CFO-based MCPCC indicates superior resilience against wind-induced disturbances and an extended hovering time.

The error between the desired pitch torque and the actual pitch torque is illustrated in Fig. 13. When the output torque is zero, it implies that the QUAV is in a state of absolute equilibrium, indicating no deviation torque in its pitch channel. Under levels 1 and 2, the similarity in deviation torque between the two methods is attributed to their comparable control performance. At level 3, IESO-based MCPCC suffers severe torque deviation, ultimately leading to loss of control. However, the loss of control in the CFO-based MCPCC is only manifested during level 5.

4.2.2. *Fixed-point hovering anti-wind disturbance experiment*

The LADRC, NLADRC, NLMPC and IESO-based MCPCC are compared with the proposed method. The wind direction of the industrial fan aligns with the x-axis of the QUAV system. The fan is positioned at a horizontal distance of 1 m from the QUAV. The center height of the industrial fan is 0.9 m. The wind velocity of levels 1, 2 and 3 is measured as 3.6, 4.5 and

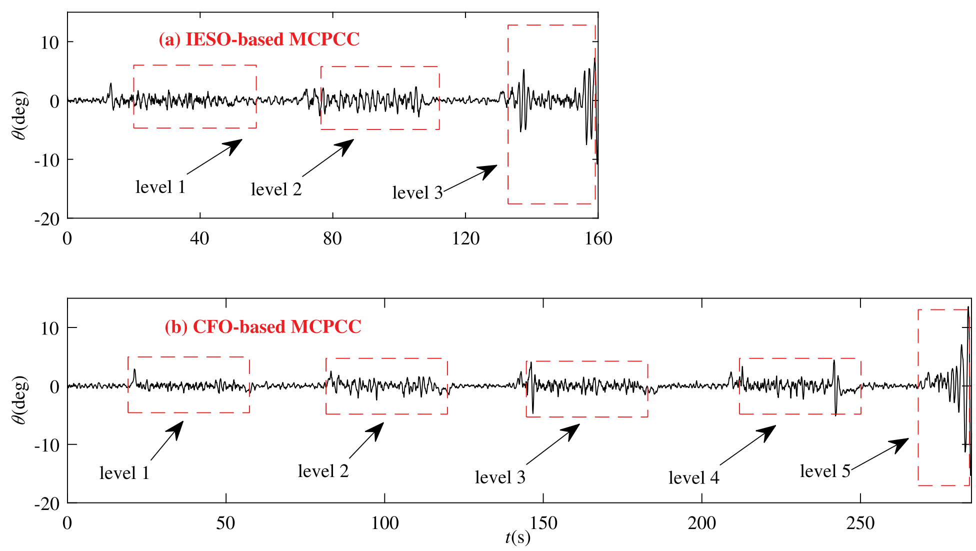

Fig. 11. Control performance of pitch under different methods.

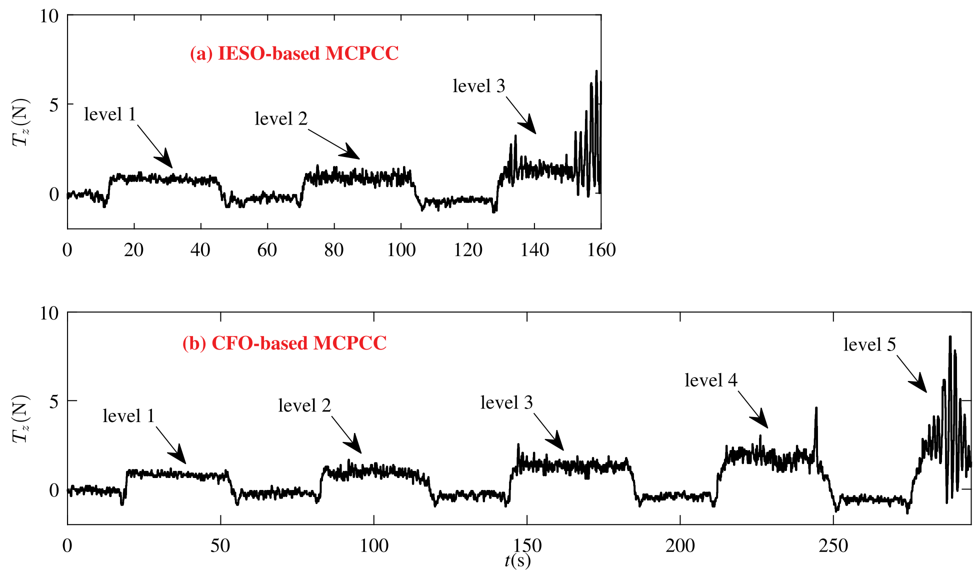

Fig. 12. Lift forces measured by a force sensor.

5.5 m/s, respectively. When the QUAV is subjected to a wind disturbance, a view of the change in the position of the windward side is presented in Fig. 14.

A comparative analysis of the horizontal control performance under different approaches is depicted in Fig. 15. LADRC, NLADRC, NLMPC and IESO-based MCPCC exhibit significant position oscillation issues. However, the proposed control approach consistently remains within the circle with a radius of 0.05 m. The results show that the proposed method has a stronger resistance to wind disturbance than other methods.

The height control performance of the five methods is demonstrated in Fig. 16. The results indicate that CFO-based MCPCC outperforms the other methods in wind disturbance suppression, without exhibiting any sharp fluctuations.

The maximum error and the mean absolute error of the five methods are presented in Table 5. The results indicate that the proposed CFO-based MCPCC method achieves the best control performance.

4.2.3. *Position tracking experiment under regional wind condition*

Under a level-2 (4 m/s) wind disturbance, the three-dimensional trajectory of the five methods is presented

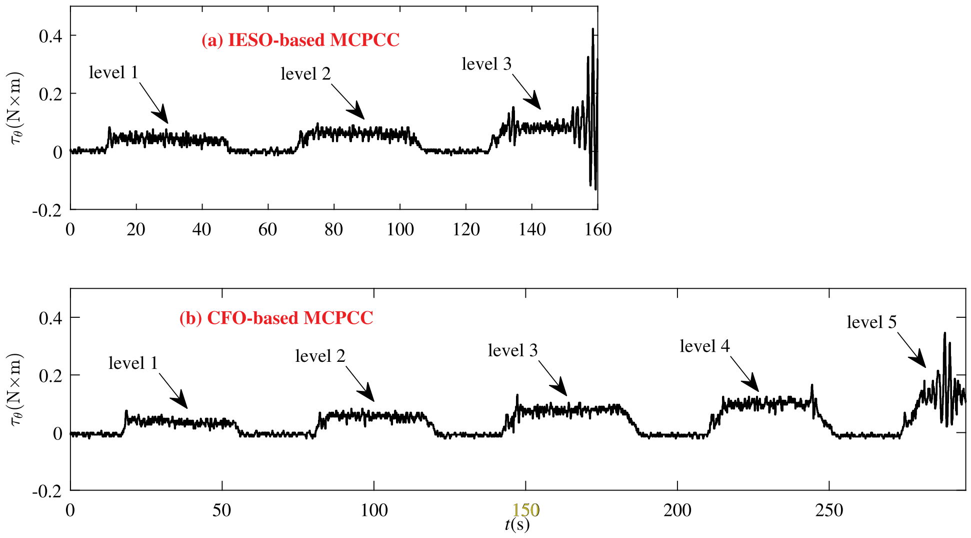

Fig. 13. Torque errors of pitch.

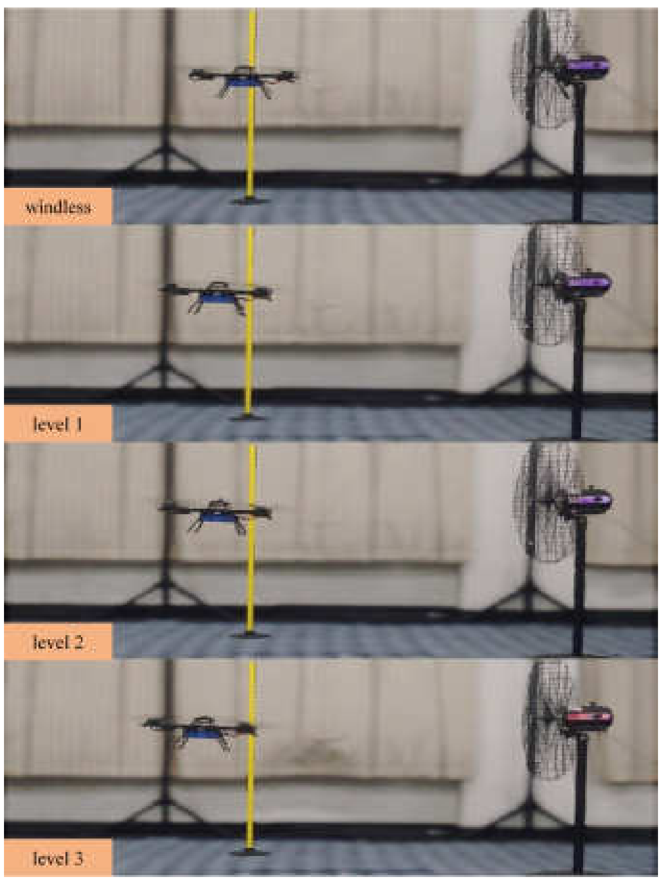

Fig. 14. A view of the change on the windward side based on CFO-based MCPCC.

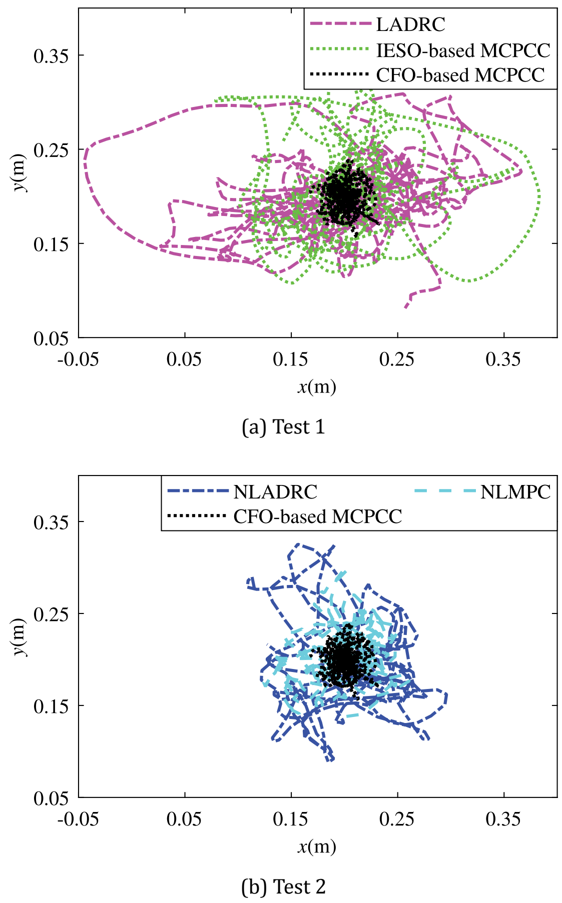

Fig. 15. Horizontal position response under wind disturbance.

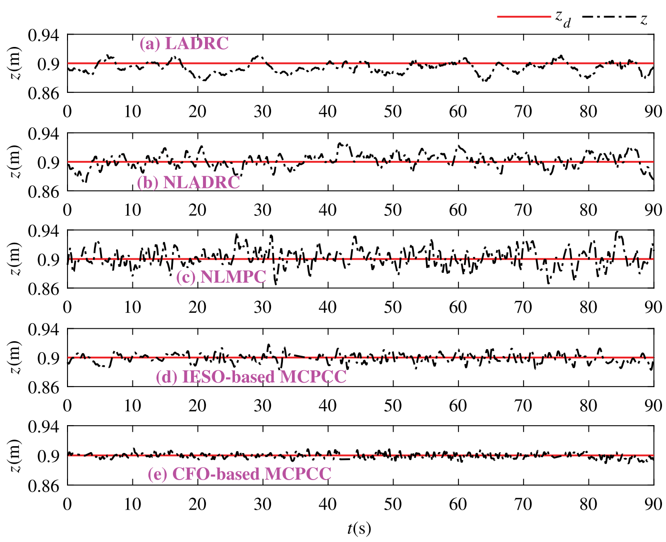

Fig. 16. Vertical control performance under wind disturbance.

Table 5. Comparison of hovering errors.

Methods	Max errors x, y, z	MAEs x, y, z
LADRC	0.244, 0.12, 0.024	0.028, 0.045, 0.011
NLADRC	0.096, 0.125, 0.0302	0.036, 0.038, 0.007
NLMPC	0.076, 0.101, 0.038	0.023, 0.024, 0.015
IESO-based MCPCC	0.183, 0.153, 0.019	0.033, 0.038, 0.005
CFO-based MCPCC	0.032, 0.043, 0.011	0.012, 0.008, 0.003

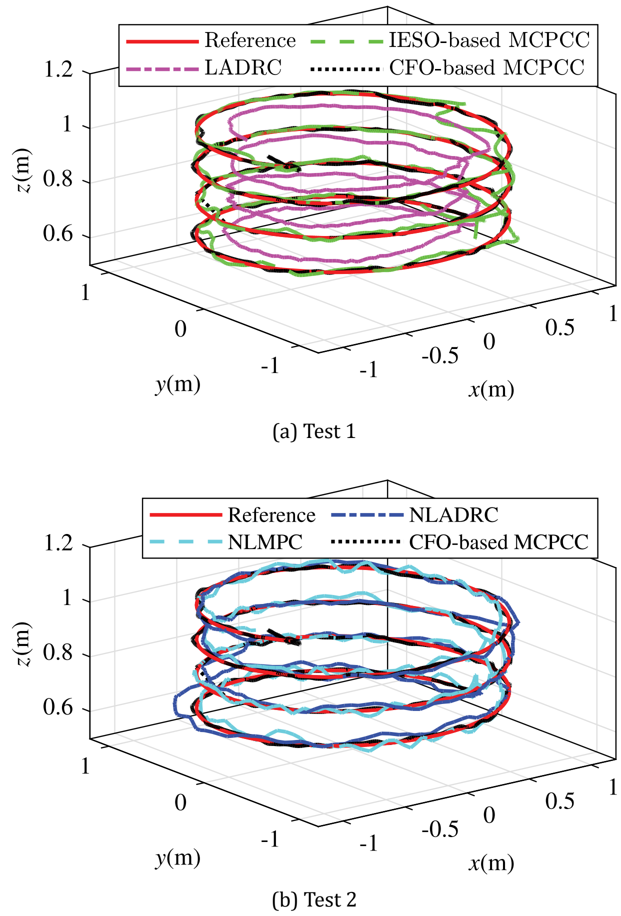

Fig. 17. Tracking trajectory under the constant wind.

in Fig. 17. From Fig. 17(a), the LADRC method shows significant deviations from the desired trajectory. By analyzing Figs. 17(a) and 17(b) together, the trajectories of IESO-based MCPCC, NLADRC and NLMPC fluctuate around the desired trajectory. However, the CFO-based MCPCC closely follows the desired trajectory with high accuracy. The RMSEs of LADRC, NLADRC, NLMPC, IESO-based MCPCC and CFO-based MCPCC are 0.374, 0.157, 0.136, 0.097 and 0.052, respectively. The results demonstrate that the CFO-based MCPCC achieves the highest tracking accuracy under steady wind conditions.

4.2.4. *Position tracking experiment with variable wind disturbance condition*

The region wind disturbance is added to the left-hand side of the trajectory. The tracking performance of LADRC, NLADRC, NlMPC, IESO-based MCPCC and CFO-based MCPCC is compared. The QUAV tracks its desired trajectory for three complete revolutions, with each revolution completed corresponding to an increment of one level in fan level. The fan is fixed where the shortest distance to the reference trajectory on the upwind side is 1 m.

The tracking performance of the above methods under the influence of regional wind is demonstrated in Fig. 18. The tracking trajectories of LADRC and NLADRC are closer to the desired trajectories on the no-wind side than on the windy side, which indicates that the two methods have poor wind disturbance resistance. The tracking trajectories of IESO-based MCPCC, NLMPC fluctuate around the desired trajectory. However, the proposed CFO-based MCPCC has the least oscillation compared to the above four methods. In addition, the RMSEs of LADRC, NLADRC, NLMPC, IESO-based MCPCC and CFO-based MCPCC are 0.203, 0.138, 0.128, 0.089 and 0.05, respectively. Therefore, the CFO-based MCPCC demonstrates the strongest wind disturbance rejection capability and achieves the highest control accuracy.

Remark 4. Under identical tracking trajectories and heightened wind disturbances, the proposed method exhibits significantly superior tracking performance compared to [23], demonstrating enhanced resistance to aerodynamic disturbances.

The wind disturbance comparison experiments compare the LADRC, NLADRC, NLMPC, IESO-based MCPCC and

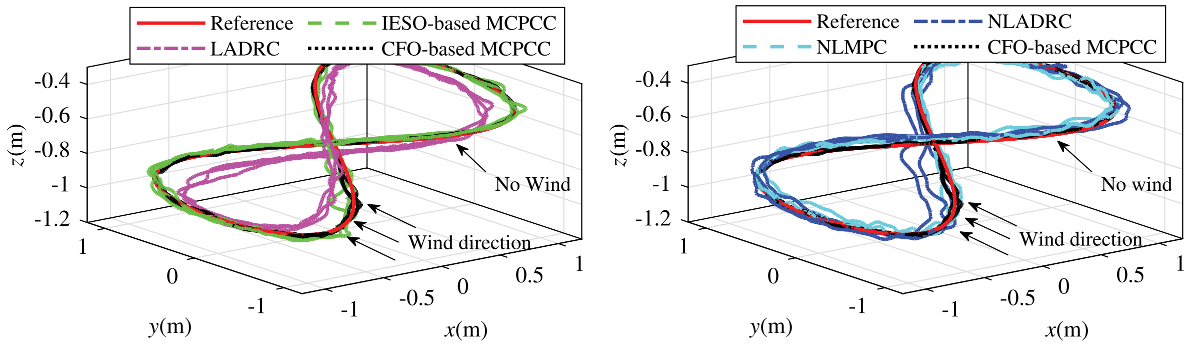

(a) Test 1

(b) Test 2

Fig. 18. Tracking trajectory with variable wind.

proposed method, respectively. The wind disturbance experiments primarily encompass attitude stabilization, fixed-point hovering, and trajectory tracking. The results demonstrate that the proposed method can realize trajectory tracking with high accuracy under different wind disturbances.

5. Conclusion

This paper proposed an active disturbance suppression method to address the challenges posed by unknown payloads and varying external disturbances in real flight for QUAVs. Model compensation pole configuration control (MCPCC) represents an inclusive control framework comprising a high-precision compensation function observer (CFO) for estimation, known model information, and derivatives of desired signals. The CFO is utilized to estimate unmodeled dynamics and external disturbances, feeding these estimates forward to the controller to counteract their effects. By leveraging known model information, the controller alleviates the burden on the observer. Controller gains are determined through pole configuration, imparting clear physical significance to parameters and thereby reducing tuning complexities. The feedback linearization of the closed-loop system is achieved by combining the derivatives of the introduced desired signal, the known model and the compensation of the unknown disturbances, and the linearised system is asymptotically stable. The framework involving CFO, HOD, pole configuration methods and known model information exhibits considerable flexibility and can be substituted at will. Under conditions of unknown payload and wind disturbances, this paper compares the performance of LADRC, NLADRC, NLMPC, IESO-based MCPCC and CFO-based MCPCC in disturbance rejection and trajectory tracking. The results indicate that the CFO-based MCPCC significantly outperforms other approaches in terms of control accuracy and disturbance rejection capability.

Future work will focus on applying this methodology to formation control and disturbance modeling for QUAVs.

Acknowledgment

This work was supported in part by the Natural Science Foundation of Tianjin City under Grant 23JCQNJC00660, and the National Natural Science Foundation of China under Grant 62303350.

ORCID

Kuo Li
https://orcid.org/0009-0004-9898-7188
Guoyuan Qi
https://orcid.org/0000-0002-0059-4879
Kun Wang
https://orcid.org/0000-0001-9253-8606
Jianbing Hu
https://orcid.org/0009-0005-4092-1079
Xia Li
https://orcid.org/0000-0002-0820-1347
Zengqiang Chen
https://orcid.org/0000-0002-1415-4073

References

[1] Z. Feng, J. Chen, W. Xiao, J. Sun, B. Xin and G. Wang, Learning hybrid policies for MPC with application to drone flight in unknown dynamic environments, *Unmanned Syst.* **12**(02) (2024) 429–441.
[2] T. Li, Y. Wan, M. Liu, S. Li, M. Pinheiro, C. He and F. Lewis, Estimation of random mobility models with application to unmanned aerial vehicles, *Unmanned Syst.* **12**(02) (2024) 391–408.
[3] K. Klausen, T. Fossen and T. Johansen, Nonlinear control with swing damping of a multirotor UAV with suspended load, *J. Intell. Robot. Syst.* **88**(2–4, 1, SI) (2017) 379–394.
[4] M. Guerrero-Sánchez, D. Mercado-Ravell, R. Lozano and C. Garcia-Beltran, Swing-attenuation for a quadrotor transporting a cable-suspended payload, *ISA Trans.* **68** (2017) 433–449.
[5] M. Guerrero-Sánchez, O. Hernández-González, C. G.-B. R. Lozano, G. Valencia-Palomo and F. López-Estrada, Energy-based control and LMI-based control for a quadrotor transporting a payload, *Mathematics* **7**(11) (2019) 1090.

[6] M. Guerrero-Sánchez, O. Hernández-González, G. Valencia-Palomo, D. Mercado-Ravell, F. López-Estrada and J. Hoyo, Robust IDA-PBC for under-actuated systems with inertia matrix dependent of the unactuated coordinates: Application to a UAV carrying a load, *Nonlinear Dyn.* **105** (2021) 1–14.
[7] J. Wang, X. Yuan and B. Zhu, Geometric control for trajectory-tracking of a quadrotor UAV with suspended load, *IET Control Theory Appl.* **16**(12) (2022) 1271–1281.
[8] E. C. J. Zhang and T. Chai, Robust fault-tolerant dynamic positioning of marine surface vessels with prescribed performance, *IEEE Trans. Intell. Transp. Syst.* **25**(12) (2024) 20950–20959.
[9] J. D. J. Zhang and T. Chai, Fault-tolerant prescribed performance control of wheeled mobile robots: A mixed-gain adaption approach, *IEEE Trans. Autom. Control* **69**(8) (2024) 5500–5507.
[10] B. Ma, Z. Liu, Q. Dang, W. Zhao, J. Wang, Y. Cheng and Z. Yuan, Deep reinforcement learning of UAV tracking control under wind disturbances environments, *IEEE Trans. Instrum. Meas.* **72** (2023) 2510913.
[11] T. Huang, D. Huang, Z. Wang, X. Dai and A. Shah, Generic adaptive sliding mode control for a quadrotor UAV system subject to severe parametric uncertainties and fully unknown external disturbance, *Int. J. Control Autom. Syst.* **19**(2) (2021) 698–711.
[12] Z. Jia, J. Yu, Y. Mei, Y. Chen, Y. Shen and X. Ai, Integral backstepping sliding mode control for quadrotor helicopter under external uncertain disturbances, *Aerosp. Sci. Technol.* **68** (2017) 299–307.
[13] K. Guo, J. Jia, X. Yu, L. Guo and L. Xie, Multiple observers based anti-disturbance control for a quadrotor UAV against payload and wind disturbances, *Control Eng. Pract.* **102** (2020) 104560.
[14] J. Han, From PID to active disturbance rejection control, *IEEE Trans. Ind. Electron.* **56**(3) (2009) 900–906.
[15] M. Wang, H. Liang, Y. Pan and X. Xie, A new privacy preservation mechanism and a gain iterative disturbance observer for multiagent systems, *IEEE Trans. Network Sci. Eng.* **11**(1) (2024) 392–403.
[16] Q. Zhong and D. Rees, Control of uncertain LTI systems based on an uncertainty and disturbance estimator, *J. Dyn. Syst. Meas. Control* **126**(4) (2005) 905–910.
[17] H. Sira-Ramirez and M. Antonio Oliver–Salazar, On the robust control of buck-converter dc-motor combinations, *IEEE Trans. Power Electron.* **28**(8) (2013) 3912–3922.
[18] C. Johnson, Optimal control of the linear regulator with constant disturbances, *IEEE Trans. Autom. Control* **13**(4) (1968) 416–421.
[19] K. Zhao, J. Zhang, D. Ma and Y. Xia, Composite disturbance rejection attitude control for quadrotor with unknown disturbance, *IEEE Trans. Ind. Electron.* **67**(8) (2020) 6894–6903.
[20] Y. Zhang, Z. Chen, X. Zhang, Q. Sun and M. Sun, A novel control scheme for quadrotor UAV based upon active disturbance rejection control, *Aerosp. Sci. Technol.* **79** (2018) 601–609.
[21] J. Yang, S. Li and X. Yu, Sliding-mode control for systems with mismatched uncertainties via a disturbance observer, *IEEE Trans. Ind. Electron.* **60**(1) (2013) 160–169.
[22] J. Back and H. Shim, Adding robustness to nominal output-feedback controllers for uncertain nonlinear systems: A nonlinear version of disturbance observer, *Automatica* **44**(10) (2008) 2528–2537.
[23] X. Zhang, Y. Zhuang, X. Zhang and Y. Fang, A novel asymptotic robust tracking control strategy for rotorcraft UAVs, *IEEE Trans. Autom. Sci. Eng.* **20**(4) (2023) 2338–2349.
[24] B. Ren, Q. Zhong and J. Dai, Asymptotic reference tracking and disturbance rejection of UDE-based robust control, *IEEE Trans. Ind. Electron.* **64**(4) (2017) 3166–3176.
[25] M. Guerrero-Sánchez, O. Hernández-González, G. Valencia-Palomo, F. López-Estrada, A. Rodríguez-Mata and J. Garrido, Filtered observer-based IDA-PBC control for trajectory tracking of a quadrotor, *IEEE Access* **9** (2021) 114821–114835.
[26] X. Shao, Q. Meng, J. Liu and H. Wang, Rise and disturbance compensation based trajectory tracking control for a quadrotor UAV without velocity measurements, *Aerosp. Sci. Technol.* **74** (2018) 145–159.
[27] Z. Gao, Scaling and bandwidth-parameterization based controller tuning, in *Proc.* 2003 *American Control Conf.* (2003), pp. 4989–4996.
[28] Y. Cao, Q. Zhao, Y. Ye and Y. Xiong, ADRC-based current control for grid-tied inverters: Design, analysis, and verification, *IEEE Trans. Ind. Electron.* **67**(10) (2020) 8428–8437.
[29] Z. Pu, R. Yuan, J. Yi and X. Tan, A class of adaptive extended state observers for nonlinear disturbed systems, *IEEE Trans. Ind. Electron.* **62**(9) (2015) 5858–5869.
[30] M. Ran, J. Li and L. Xie, A new extended state observer for uncertain nonlinear systems, *Automatica* **131** (2021) 109772.
[31] B. Qin, H. Yan, H. Zhang, Y. Wang and S. Yang, Enhanced reduced-order extended state observer for motion control of differential driven mobile robot, *IEEE Trans. Cybern.* **53**(2) (2023) 1299–1310.
[32] X. Li, G. Qi, X. Guo, Z. Chen and X. Zhao, Improved high order differential feedback control of quadrotor UAV based on improved extended state observer, *J. Franklin Inst.* **359**(9) (2022) 4233–4259.
[33] G. Qi, X. Li and Z. Chen, Problems of extended state observer and proposal of compensation function observer for unknown model and application in UAV, *IEEE Trans. Syst. Man Cybern. — Syst.* **52**(5) (2022) 2899–2910.
[34] G. Qi, Z. Chen and Z. Yuan, Adaptive high order differential feedback control for inverted pendulum system, *Control Theory Appl.* **21**(5) (2004) 676–683.
[35] Q. Quan, *Introduction to Multicopter Design and Control* (Springer, Puchong, 2018).
[36] G. Qi, J. Hu, L. Li and K. Li, Integral compensation function observer and its application to disturbance-rejection control of QUAV attitude, *IEEE Trans. Cybern.* **54**(7) (2024) 4088–4099.
[37] B. Liu, Y. Wang, O. Mofid, S. Mobayen and M. H. Khooban, Barrier function-based backstepping fractional-order sliding mode control for quad-rotor unmanned aerial vehicle under external disturbances, *IEEE Trans. Aerosp. Electron. Syst.* **60**(1) (2024) 716–728.
[38] G. Qi, J. Deng, X. Li and X. Yu, Compensation function observer-based model-compensation backstepping control and application in anti-inference of quadrotor UAV, *Control Eng. Pract.* **140** (2023) 105633.
[39] D. Hanover, P. Foehn, S. Sun, E. Kaufmann and D. Scaramuzza, Performance, precision, and payloads: Adaptive nonlinear MPC for quadrotors, *IEEE Robot. Autom. Lett.* **7**(2) (2022) 690–697.
[40] G. Tao, A simple alternative to the Barbalat lemma, *IEEE Trans. Autom. Control* **42**(5) (1997) 698.
[41] A. S. Brandao, D. Smrcka, E. Pairet, T. Nascimento and M. Saska, Side-pull maneuver: A novel control strategy for dragging a cable-tethered load of unknown weight using a UAV, *IEEE Robot. Autom. Lett.* **7**(4) (2022) 9159–9166.

Kuo Li received his B.S. degree in automation from the Shandong Technology and Business University, Yantai, China, in 2021. He is currently pursuing his M.S. degree in Control Science and Engineering at the Tiangong University, Tianjin, China. His research interests include identification, modeling, disturbance estimation, and anti-disturbance control strategies.

Guoyuan Qi received his B.S. Degree in Mathematics from the Normal University of Mudanjiang, Mudanjiang, China, in 1992, his M.S. Degree in Control Theory and Control Engineering from the Heilongjiang University, Harbin, China, in 2001, and his Ph.D. Degree in Control Theory and Control Engineering from the Nankai University, Tianjin, China, in 2004. He is Professor at the Department of Control Science and Engineering, the Tiangong University, Tianjin, where he is Chair Professor. He has authored and co-authored more than 90 journal papers. His research interests include nonlinear dynamics, modeling, and control of nonlinear systems, chaos analysis, and circuit implementation.

Kun Wang obtained her B.S., M.S. and Ph.D. Degrees from the Northeastern University, Shenyang, China, in 2012, 2014 and 2021, respectively. From 2019 to 2020, she was Visiting Scholar at the Department of Electrical Engineering, the Lakehead University, Thunder Bay, ON, Canada. She is currently at the School of Control Science and Engineering, the Tiangong University. Her current research interests include control problems in finite time control, prescribed performance control, modern communication network systems, networks traffic management, and control of QUAV and analysis.

Jianbing Hu received his M.S. Degree in Control Theory and Control Engineering, the Tiangong University, Tianjin, China, in 2018, where he is currently pursuing his Doctoral degree in Mechanical Engineering. His research interests include modeling, identification, dynamical analysis of nonlinear systems, and disturbance rejection control strategies for unmanned aerial vehicles.

Xia Li was born in Shanxi, China, in January 1992. She received her B.S. Degree in Engineering from the Taiyuan University of Science and Technology, Taiyuan, China, in 2017, and her M.S. degree in Control Theory and Control Engineering, the Tiangong University, Tianjin, China, in 2019, and her Ph.D. degree in Mechanical Engineering, the Tiangong University, Tianjin, China, in 2024. Her research interests include modeling, control and estimation of nonlinear systems, dynamical analysis, and control strategies for unmanned aerial vehicles.

Zengqiang Chen received his B.S. Degree in Mathematics, and his M.S. and Ph.D. Degrees in Automatic Control from the Nankai University, Tianjin, China, in 1987, 1990 and 1997, respectively. He is currently Full Professor with the Department of Automation, College of Artificial Intelligence, the Nankai University. He has authored and coauthored over 200 journal papers. His main research interests include active disturbance rejection control, model-based predictive control, intelligent optimizing control and nonlinear control.